BRAIN
ORIGINAL ARTICLE

Validating visual evoked potentials as a preclinical, quantitative biomarker for remyelination efficacy

Christian Cordano,[1] Jung H. Sin,[1] Garrett Timmons,[1] Hao H. Yiu,[1] Karin Stebbins,[2] Caroline Guglielmetti,[3] Andres Cruz-Herranz,[1] Wendy Xin,[1] Daniel Lorrain,[2] Jonah R. Chan[1] and Ari J. Green[1]

Many biomarkers in clinical neuroscience lack pathological certification. This issue is potentially a significant contributor to the limited success of neuroprotective and neurorestorative therapies for human neurological disease—and is evident even in areas with therapeutic promise such as myelin repair. Despite the identification of promising remyelinating candidates, biologically validated methods to demonstrate therapeutic efficacy or provide robust preclinical evidence of remyelination in the CNS are lacking. Therapies with potential to remyelinate the CNS constitute one of the most promising and highly anticipated therapeutic developments in the pipeline to treat multiple sclerosis and other demyelinating diseases. The optic nerve has been proposed as an informative pathway to monitor remyelination in animals and human subjects. Recent clinical trials using visual evoked potential have had promising results, but without unequivocal evidence about the cellular and molecular basis for signal changes on visual evoked potential, the interpretation of these trials is constrained. The visual evoked potential was originally developed and used in the clinic as a diagnostic tool but its use as a quantitative method for assessing therapeutic response requires certification of its biological specificity. Here, using the tools of experimental pathology we demonstrate that quantitative measurements of myelination using both histopathological measures of nodal structure and ultrastructural assessments correspond to visual evoked potential latency in both inflammatory and chemical models of demyelination. Visual evoked potential latency improves after treatment with a tool remyelinating compound (clemastine), mirroring both quantitative and qualitative myelin assessment. Furthermore, clemastine does not improve visual evoked potential latency following demyelinating injury when administered to a transgenic animal incapable of forming new myelin. Therefore, using the capacity for therapeutic enhancement and biological loss of function we demonstrate conclusively that visual evoked potential measures myelin status and is thereby a validated tool for preclinical verification of remyelination.

1 Department of Neurology, Weill Institute for Neuroscience, University of California, San Francisco, San Francisco, CA 94158, USA
2 Inception Sciences, San Diego, CA 92121, USA
3 Department of Physical Therapy, University of California, San Francisco, San Francisco, CA 94158, USA

Correspondence to: Jonah R. Chan
University of California 675 Nelson Rising Lane San Francisco CA 90158, USA
E-mail: jonah.chan@ucsf.edu

Correspondence may also be addressed to: Ari J. Green
E-mail: agreen@ucsf.edu

Keywords: remyelination; visual evoked potential; demyelination; clemastine

Received January 12, 2022. Revised May 19, 2022. Accepted May 30, 2022. Advance access publication June 9, 2022

Abbreviations: CASPR = contactin associated protein; EAE = experimental autoimmune encephalomyelitis; EM = electron microscopy; OPCs = oligodendrocyte precursor cells; VEP = visual evoked potential

Introduction

Restoration of the myelin sheath is an unrealized therapeutic goal in the treatment of multiple sclerosis that promises to help with functional recovery and prevention of long-term disability. Despite the identification of potential therapeutic candidates capable of restoring myelin, we currently lack sufficiently biologically validated methods for preclinical assessment that will predict a high likelihood of clinical success. An encouraging therapeutic approach for remyelination is to enhance differentiation of the endogenous oligodendrocyte precursor cells (OPCs) into mature myelinating oligodendrocytes and thereby stimulate remyelination of demyelinated axons before neuronal substructure is permanently lost. A number of screens including one performed by our team using a micropillar platform with postnatally derived OPCs (BIMA)[1] identified compounds capable of stimulating differentiation and remyelination: the most prominent of which was the small molecule compound clemastine.[1,2] On the basis of strong cellular, molecular and *in vivo* evidence for remyelination with clemastine, we were afforded the opportunity to investigate and validate potential remyelination biomarkers in the preclinical setting using this agent. Clemastine's use as a uniquely powerful tool compound, was strengthened after completion of the first positive double-blind placebo controlled human trial for a remyelinating agent using clemastine in multiple sclerosis and visual evoked potential (VEP) as the primary outcome. In this trial, we unequivocally demonstrated improvement in long-standing latency delay on VEPs for patients during the period on treatment despite the chronicity of injury.[3] However, full assessment of the trial findings remains constrained because there is insufficient documentation of the biological effects of demyelination and remyelination in impacting VEP latency. The VEP is an electric potential recorded from the visual cortex in response to a repeating visual stimulus, allowing the evaluation of time needed for a signal to travel from the retina to the visual cortex.[4,5] As a consequence, VEP has been the primary outcome in phase-II clinical trial programmes that aim to assess remyelinating therapies.[3,6,7] However, an unequivocal quantitative relationship between VEP latency and myelin status has been lacking. Histological data assessing the direct relationship between demyelination and remyelination and latency delay are inadequate because of (i) the inaccessibility of tissue in the human disease; (ii) the lack of previous reliable well established methods for the performance of reproducible VEPs in animal models (especially mice); (iii) a historical conflation of the concepts of inflammation and demyelination when considering the biological basis of the VEP signal; and (iv) the prior absence of tool compounds capable of inducing remyelination. Histological assessments correlated with VEP animal models to date are also neither definitive nor adequately quantitative because of (i) the imputation of latencies when the VEP signal was absent[8]; (ii) the use of unreliable chemical stains for the assessment of myelin status[9–12]; and (iii) confounding issues created by the inability to uncouple demyelination, remyelination, axonal loss and inflammation.[8–10,12] Additional previous research evaluated VEPs and histology in the context of limited spontaneous, but not therapeutically enhanced, remyelination after toxic demyelination in rats (injection of lysolecithin)[13] and cats (irradiated diet).[14] By using tools that allow us to control and induce remyelination, we are able to evaluate whether putative myelin biomarkers actually measure myelin restoration. Furthermore, to help investigate and disentangle the effect of inflammation on myelin biomarkers, we undertook to assess VEP in the context of both (i) experimental autoimmune encephalomyelitis (EAE), which models myelin targeted adaptive immune-mediated demyelination; and (ii) chemical demyelinating models without targeted inflammation (i.e. cuprizone), as well as to consider the effect on VEP for assessing myelin status in the context of an animal model where no new myelin can be formed.

Materials and methods

Animal statement

All animals were maintained in barrier facilities on a 12-h light/dark cycle with food and water ad libitum. Experiments were conducted in compliance with the ARVO Statement for the Use of Animals in Ophthalmic and Vision Research.

EAE scoring

EAE mice were scored as previously described.[15]

Visual evoked potentials

Flash based binocular visual electrophysiology was performed using an Espion Diagnosys system (Diagnosys LLC) in anaesthetized mice with dilated pupils (Supplementary Fig. 1). The protocol was optimized in terms of timing, anaesthesia and preconditioning to obtain an average intra-subject variability of 0.9 ms on two different examinations performed on two different days on the same animal (data not shown). Mice were anaesthetized via intraperitoneal injection using a combination of xylazine (20 mg/ml) and ketamine (100 mg/ml) diluted in PBS administered at a dose of 0.125 ml per 20 g of mouse weight (87.5 mg/kg ketamine and 12.5 mg/kg xylazine). VEP recordings were performed in a room with low ambient light (28–32 lx). Six minutes after induction of anaesthesia (and following administration of tropicamide 1% one drop in each eye) mice were placed for 5 min within a sealed small cardboard box (12 × 12 × 16 cm). The animal was then placed and positioned on a flat surface for insertion of the 1 cm steel needle electrodes (Natus Neurology). The active electrode for the flash VEP is placed medially under the skin between the two eyes, along the sagittal suture, with the needle's tip inserted to 8 mm depth, to optimize proximity to the visual cortex. A subcutaneous needle electrode inserted just above the tip of the nose serves as reference and a needle electrode in the tail serves as the ground. Following placement of the electrodes, the dome was lowered before initiation of the recording (the positioning of the electrodes took ~1 min) and VEP stimulation and recording began precisely 13 min after administration of anaesthesia. During any remaining time from the insertion of the electrodes until initiation of recording, the animal was kept in the dark conditions created by the lowered dome. Each exam consisted of three runs, with pulse intensity 3 cd.s/m^2, frequency 1 Hz, on-time 4 ms, white pulse colour at 6500 K and 100 sweeps

per acquisition. Under these conditions, the standard VEP waveform was characterized by a prominent negative deflection after ~80 ms, which was identified as N1. By laboratory protocol, N1 was defined as the first negative deflection after 60 ms. The two most representative/reproducible waves or the most well-defined wave were used for analysis. The exam was performed by an operator blinded for mice group/genotype until performing the data analysis. The order of measurements was maintained during the described experiments.

Longitudinal VEP in EAE

C57BL/6J female mice (Jackson Laboratory, 8 weeks old on arrival) were allowed to acclimate for 1 week before induction of EAE. EAE was induced via immunization with $MOG_{35–55}$ (Genemed Synthesis) peptide emulsified in complete Freund's adjuvant (CFA) at a dose of 100 μg per mouse, followed by the administration of pertussis toxin (200 ng per mouse through intraperitoneal injection; List biological laboratories) on Days 0 and 2 post-immunization. Body weights and EAE clinical scores were assessed at least four times per week. Control mice were sham-immunized with PBS in CFA and received the same pertussis toxin dosage. Animals were assigned sequentially to treatment with clemastine or vehicle. EAE mice ($n = 6$) and sham-immunized mice ($n = 5$) underwent VEP six times over 40 days (at Days 0, 5, 10,18, 28, 40 post-immunization) (Fig. 1A) to define the relationship between EAE score and VEP.

Remyelinating treatment in EAE

C57BL/6J female mice (Envigo, 8 weeks old on arrival) were allowed to acclimate for 1 week before induction of EAE. On Day 0, $MOG_{35–55}$, (Genemed Synthesis) was solubilized in PBS at a 2 mg/ml concentration. Incomplete Freund's adjuvant (BD) was made complete by the addition of 4 mg/ml H37RA (BD). A suspension of MOG in IFA/H37RA was prepared by mixing 1:1. During the immunization, each mouse was injected subcutaneously in the dorsal subscapular and lower lumbar regions with 100 μl, divided over four sites, followed by the intraperitoneal administration of pertussis toxin (200 ng) per mouse on Day 0 and Day 2 post-immunization. Vehicle ($n = 15$ mice) or clemastine ($n = 15$ mice) (10 mg/kg prepared in 20% kleptose) was dosed *per os* once daily beginning on Day 0. Body weights and clinical scores were assessed daily. Treatment was administered prophylactically to ensure axonal preservation during acute inflammation[16] and to treat the pre-symptomatic latency changes. VEPs were performed weekly over 28 days comparing vehicle-treated EAE, clemastine-treated EAE and sham-immunized mice ($n = 13$ mice).

Remyelinating treatment in a toxic demyelinating model

C57BL/6J female mice (Envigo, 6–7 weeks of age on arrival) were allowed to acclimate for at least 1 week before being placed on 0.2% cuprizone diet (Harlan, cuprizone diet 0.2%, pellet). After 5 weeks of cuprizone diet, animals were returned to standard rodent chow (Harlan, 18% global rodent diet) for 2 weeks to allow spontaneous remyelination to occur. Mice were dosed with clemastine from Sigma Aldrich once daily *per os* via gavage at 10 mg/kg ($n = 8$ mice) or vehicle ($n = 12$) (0.5% methyl cellulose) *per os* at 10 ml/kg. Daily dosing began on the same day mice were placed back on regular rodent chow diet and continued dosing for up to 14 days. VEPs were performed weekly (three times) beginning the day mice were placed back on a regular rodent chow diet.

VEP in *Myrf* conditional knockout

Mouse lines carrying 'floxed' alleles of *Myrf* on a *NG2creERT* background (courtesy of the Ben Emery Laboratory, OHSU) (JAX 008538) were used to induce conditional knockout of the *Myrf* gene in NG2-expressing OPCs. Then 8-week-old female $Myrf^{flox/flox}$ mice ($n = 11$) and *NG2-CreER*;$Myrf^{flox/flox}$ mice ($n = 10$) were administered by oral gavage a tamoxifen solution prepared by dissolving tamoxifen (Sigma Aldrich) in corn oil at 40 mg/ml by sonication for 1 h at 21°C (each dose being 300 mg tamoxifen/kg body weight) for four consecutive days starting 7 days before the start of the cuprizone diet. Toxic demyelination was induced as already described in the section 'remyelinating treatment in a toxic demyelinating model'. After 5 weeks on the cuprizone diet, animals were returned to standard rodent chow (Harlan, 18% global rodent diet) for up to 2 weeks and treated via gavage either with clemastine (five mice for each group) or vehicle (six mice *NG2-CreER* $Myrf^{flox/flox}$ and five mice $Myrf^{flox/flox}$) for 14 days as already described in the section 'remyelinating treatment in EAE'. VEPs were measured at two time points: (i) at discontinuation of the cuprizone diet; and (ii) 2 weeks after discontinuation.

Immunohistochemistry

Mice were placed in a CO_2 chamber until fully unconscious and intracardially perfused with cold 4% paraformaldehyde in 0.1 M PBS at pH 7.4. Optic nerves were dissected *in situ* proximally behind the orbitae and distally before the optic chiasm. Dissected optic nerves were post-fixed for 12 h in paraformaldehyde 4% and followed by a 30% sucrose in 0.1 M PBS for 48 h before embedding in Tissue-Tek OCT (Sakura) and long-term storage at −80°C. Immunohistochemistry was performed on 16 μm longitudinal sections. Sections were rinsed in PBS and blocked with 10% serum of species in which secondary antibodies were raised. Primary antibody incubations were carried out overnight at 4°C in PBS containing 0.01% Triton-X normal goat serum. IHS was performed using rabbit anti-CASPR (1:1000, Abcam, ab34151) as primary antibody. Gt-αRb (1:1000)—488 was used as secondary antibody. Negative control sections without primary antibodies were processed in parallel. Alexa-Fluor tagged secondary antibodies (Invitrogen) were used for primary antibody detection at room temperature. Images were acquired using an upright Axio Imager 2 microscope (Carl Zeiss Microscopy) and processed using ImageJ software (NIH).

CASPR density quantification

The z-stacked images acquired at ×400 total magnification (objective lens of 40×) were then processed through ImageJ software. For each z-stack, four adjacent images with the highest quality were chosen then merged together by adjusting for maximum intensity. Individual nodes were identified by the presence of two punctate fluorescent dots, in close proximity to one another, that are separated by a small, non-fluorescent space and aligned along a similar axis (Supplementary Fig. 2). Using the MTrackJ plugin, discernible paranode structures within randomly selected areas within each sample were counted to calculate the density (paranode count/mm^2) in millimetres squared.

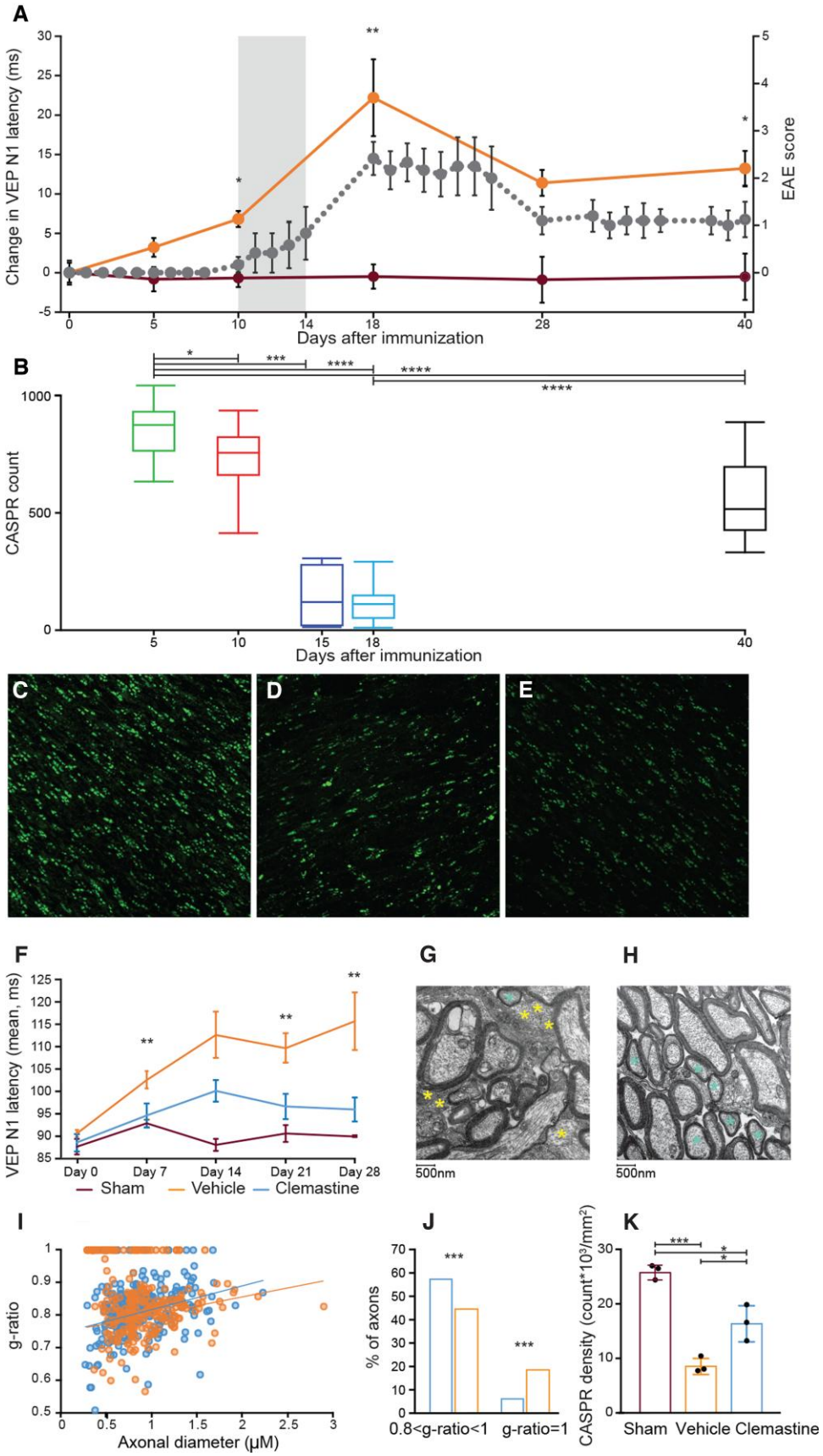

Figure 1 Effect of clemastine on remyelination in the EAE model. **(A)** Prolongation of VEP latency precedes clinical onset (grey area) of EAE (grey dots represent EAE score). VEP latency (in orange) is delayed 5 days post-immunization when compared with sham-immunized mice (wine red).

(Continued)

Electron microscopy

Mice were placed in a CO_2 chamber until fully unconscious and intracardially perfused with electron microscopy (EM) fixative (5% glutaraldehyde, 4% paraformaldehyde in 0.15 M sodium cacodylate, pH 7.4). Samples were immersed in modified Karnovsky's fixative (2.5% glutaraldehyde and 2% paraformaldehyde in 0.15 M sodium cacodylate buffer, pH 7.4) for at least 4 h, post-fixed in 1% osmium tetroxide in 0.15 M cacodylate buffer for 1 h and stained *en bloc* in 2% uranyl acetate for 1 h. Samples were dehydrated in ethanol, embedded in Durcupan epoxy resin (Sigma Aldrich), sectioned at 50 to 60 nm on a Leica UCT ultramicrotome and picked up on Formvar and carbon-coated copper grids. Sections were stained with 2% uranyl acetate for 5 min and Sato's lead stain for 1 min. Grids were viewed using a JEOL 1200EX II transmission electron microscope and photographed using a Gatan digital camera), or viewed using a Tecnai G2 Spirit BioTWIN transmission electron microscope equipped with an Eagle 4k HS digital camera (FEI). The g-ratios were calculated by measuring the ratio of axonal diameter and the diameter of the outer myelin sheath. G-ratio values between 0.8 and 0.99 were considered remyelinating axons.

Statistical analysis

Statistical analyses were performed using GraphPad (PRISM v.7). The sample size for the experiments was decided based on pilot study data. Animals with eye abnormalities were not included in the experiments. Given that the mice from each group were either from the same inbred mouse line or were otherwise genetically identical, no randomization process was used. All the animal and available data points were included in the analysis. Spearman's rho (ρ) was used to determine the correlation between EAE score and VEP latency. A two-tailed Student's *t*-test was used to determine statistical significance between groups in terms of CASPR staining quantification; the Mann–Whitney test was used to determine statistical significance when groups were compared in terms of VEP latencies, while the chi-squared test was used to compare groups in terms of g-ratios. Statistical significance was expressed as $^{*}P < 0.05$, $^{**}P < 0.01$ and $^{***}P < 0.001$. The investigators were blinded to the allocation of compounds until the final statistical analysis. Age-matched C57BL/6 mice were randomly allocated to either control or treatment group for all the experiments.

Study approval

All protocols were approved by the Institutional Animal Care and Use Committee of the University of California, San Francisco.

Data availability

All data and materials other than animal models that are not intellectual property of the laboratory used in the analysis are available to any researcher for purposes of reproducing or extending the analysis.

Results

VEP N1 latency is delayed in early experimental autoimmune encephalomyelitis

Mice with MOG-induced EAE showed substantial latency delay of the first negative deflection (N1) (directly analogous to p100 in humans) including the period before detectable signs of weakness at 5 and 10 days post-immunization (Fig. 1A). In symptomatic animals, N1 latency had a strong correlation with EAE score ($\rho = 0.84$, $P < 0.0001$) (Supplementary Fig. 3), but importantly latency delays were detectable earlier, illustrating that VEPs have superior sensitivity to traditional EAE scores. Peak latency delay was seen around the peak of motor impairment (Day 18 post-immunization) followed by an incomplete recovery over 10 days.

VEP N1 latency mirrors longitudinal quantitative assessment of myelin status

Direct quantifiable methods to visualize myelin at high spatial resolution is limited by numerous factors. Despite the recent identification of promising methods for myelin quantification, such as PET,[17] two photon live-imaging techniques,[18] optical coherence microscopy,[19] third harmonic generation microscopy,[20] spectral confocal reflectance microscopy,[21] coherent anti-Stokes Raman scattering microscopy[22] and the stochastic gene activation with regulated sparseness reporter mouse,[23] standard immunohistochemical stains are still non-quantitative and rely on detecting the presence of myelin proteins. Fluorescence intensity does not correlate to the 'amount' of myelin present either in terms of length or area myelinated or in terms of quantity of myelin overall. Furthermore, historical but still commonly used chemical methods for myelin staining are unreliable, due to their tremendous variability and dependence on technical factors.[24] For this reason, previous histological assessments of myelination correlated with VEP animal models have been neither definitive nor adequately quantitative.[9–12]

A central feature of myelin is the presence of the nodes of Ranvier with clustering of ion channels for the depolarization of the axon. The formation of the paranode is driven by contact-mediated mechanisms depending on specific axoglial interaction and follows and requires the presence of flanking internodes of myelin.[25] We therefore used a method to stain for and count doublets of the paranodal contactin associated protein (CASPR) as a quantitative technique for immunohistochemically assessing optic nerve myelination. The VEP changes in latency mirrored longitudinal quantitative measurement of CASPR count, showing a progressive drop of the paranodes count starting at Day 10 post-immunization and culminating at peak of disease (Day 18 post-immunization). In conjunction with the lack of recovery of N1 latency delay, CASPR quantification showed incomplete recovery of optic nerve myelination at Day 40 post-immunization (Fig. 1B–E).

Figure 1 Continued
N1 latency increases through Day 18 with subsequent improvement. (**B**) Optic nerve CASPR quantification in EAE mice. This mirrors **A** showing the histopathological correlate of N1 delay. (**C–E**) Examples of CASPR doublets from healthy optic nerve (**C**) and EAE mice 15 days and 40 post-immunization. (**D** and **E**). (**F**) Effect of clemastine on VEP latency in EAE mice. (**G** and **H**) Examples of ON EM micrographs from EAE mice treated with vehicle (**G**) and clemastine (**H**) 28 days post-immunization. Three mice were analysed per group. Note unmyelinated axons (yellow asterisk) and remyelinating axons (light blue asterisk). (**I**) G-ratios of optic nerve axons 28 days post-immunization. (**J**) Quantification of unmyelinated (g-ratio = 1) and remyelinating (0.8 < g-ratio < 1) axons. (**K**) CASPR quantification shows improvement of paranodal density (count × 10^3/mm^2) in mice treated with clemastine compared with vehicle. Error bars describe SEM for latency change and EAE score graphs, SD for the other graphs.

Clemastine treatment improves VEP N1 latency in EAE and increase the number of remyelinated axons within the optic nerve

Clemastine was identified by our group as a tool compound able to induce differentiation of OPCs and remyelination[1] and can improve p100 latency when administered in relapsing-remitting patients with multiple sclerosis without recent relapses.[3] Because of the inaccessibility of tissue in the human disease, it has so far been impossible to demonstrate that the visual function improvement following treatment we described in patients with multiple sclerosis was induced by actual tissue repair. To histologically assess the direct relationship between remyelination and latency delay we administered clemastine in EAE mice. We documented that clemastine induced remyelination corresponded with both latency recovery (Fig. 1F) and an increase in paranodal density in the optic nerve (Fig. 1K) ($P = 0.02$). Clemastine, administered daily via gavage at the dosage of 10 mg/kg, was associated with improved N1 latency, performed on a weekly basis (Fig. 1F) ($P = 0.003$ at Day 7 post-immunization, $P = 0.07$ at Day 14, $P = 0.002$ at Day 21, $P = 0.008$ at Day 28). Ultrastructural evidence also demonstrated an increase in remyelinated axons ($P < 0.001$) and decrease in unmyelinated axons ($P < 0.001$), in the ONs of treated mice assessed via EM [remyelination classified as a g-ratio between 0.8 and 1 (Fig. 1G–J)].

VEP N1 latency is delayed in the cuprizone model of demyelination and clemastine speeds up remyelination

To dissect out the inflammation effect on VEP from the effect of myelin loss and remyelination, we used the cuprizone model of demyelination. Cuprizone administration induces demyelination with minimal clinical deficits. In this model, inflammation (microgliosis and astrogliosis) is reactive to OL death and the presence of myelin debris, and inflammation is therefore not a driving force but a response to injury. It has been previously shown that cuprizone diet induces myelin loss and potassium channel displacement within the ON.[26–28] N1 latency after 5 weeks of cuprizone diet showed an evident delay when compared with healthy mice matched for sex and age (healthy, average N1 = 86 ms, SD 6.7; cuprizone diet: average N1 = 101.1 ms, SD 14.5; $P = 0.005$; Fig. 2A). Clemastine (10 mg/kg) administered after discontinuation of the cuprizone diet enhanced VEP latency recovery, with a shorter N1 latency in clemastine-treated mice versus vehicle-treated mice after 2 weeks of treatment (Fig. 2C) ($P = 0.007$). ONs from clemastine-treated animals evaluated by immunohistochemistry and EM also showed a significant increase in the number of paranodes (Fig. 2B) ($P = 0.03$) and increased number of remyelinating axons (Fig. 2D–G) ($P < 0.01$).

VEP N1 recovery after demyelination is absent in OPC-specific *Myrf* knockout mice

Having shown that clemastine administration induces an improvement in VEP latency following administration to animals with both inflammatory and non-inflammatory demyelination, we still required evidence that remyelinating agents generate their observed improvement in VEP latency solely via the restoration of myelin (and not via some other separate effect). Furthermore, we aimed to assess whether VEP latency can recover at all in the absence of the formation of new myelin. To answer these questions, we used a transgenic animal model with inability to form new myelin, previously described by McKenzie *et al.*[29] Mice with an OPC-specific conditional, cre-inducible knockout of the transcription factor myelin regulatory factor (*Myrf*) (*NG2-creER;Myrf*$^{flox/flox}$) cannot form new myelin on recombination but pre-existing myelin is unaltered.[29] To ensure that deletion of *Myrf* was long-lasting and efficient, we induced recombination at postnatal Days 9–13 with tamoxifen and imaged the visual cortex at postnatal Days 28 and 180. In both cases, deletion of *Myrf* from OPCs significantly halted the progression of oligodendrogenesis and myelination without significant recovery (Supplementary Fig. 4).

We assessed VEPs comparing *Myrf*$^{flox/flox}$ versus *NG2-creER*; *Myrf*$^{flox/flox}$ following the administration of tamoxifen in adult animals 2 weeks after cuprizone-induced demyelination (Fig. 3). Animals with the OPC-specific knockout of *Myrf* showed an absence of improvement in N1 latency delay after cessation of cuprizone chow—thereby documenting that VEP latency recovery is directly tied to the capacity to remyelinate (Fig. 2H). We then compared *Myrf*$^{flox/flox}$ and *Myrf icKO* following treatment with both clemastine and vehicle. In the absence of the capacity to remyelinate clemastine induced no improvement in VEP latency (Fig. 2H). In this experiment, the *Myrf*$^{flox/flox}$ NG2creERT negative controls did not display a statistically significant difference with or without clemastine treatment due to smaller numbers of mice in the cohort than in the previously described experiment (Fig. 2C).

Discussion

EAE is an animal model of multiple sclerosis that results in the inflammatory demyelination observed in the disease.[30] Most frequently, EAE is induced via immunization with $MOG_{35–55}$ peptide and is characterized by a variable onset of ascending motor impairment progressing to paraparesis or tetraparesis in a significant number of animals. Animals also exhibit variable but frequently incomplete recovery and evidence of myelitis and optic neuritis.[30] Animals are assessed for deficits using a scoring system that is largely subjective and although assigned a numerical value actually represents a categorical assessment of functional impairment. The observed variability in disease severity and onset between animals and between experiments is predicated by a number of different factors including variation in immune response and various laboratory-specific conditions but is contributed to by the insensitive and non-quantitative methods we use for assessment.[31] This makes investigating and understanding the biology of EAE including immune processes, induction of CNS injury and any subsequent recovery more challenging and prone to bias. We therefore sought to develop a reproducible and reliable electrophysiological method to capture the first signs of functional impairment in EAE that is also capable of quantitatively tracking longitudinal injury and improvement. We sought to exploit the visual system and to compare results to our previously conducted clinical trial. Therefore, we developed a method using subcutaneous needle electrodes and carefully timed anaesthesia for reliable, repeatable VEP waveforms. We have biologically validated VEP as a quantitative outcome measure for remyelination. We found that VEP N1 in EAE is delayed earlier than the first detectable clinical signs of weakness used to quantify the EAE score, suggesting that VEP is a more sensitive and quantitative way to measure clinical deficit in this model. The previously described limits of the EAE score makes understanding which component of immunological activation or resulting injury yields changes in EAE score difficult, while the use of VEP N1 latency could help to better understand the causes of disease variability. Our

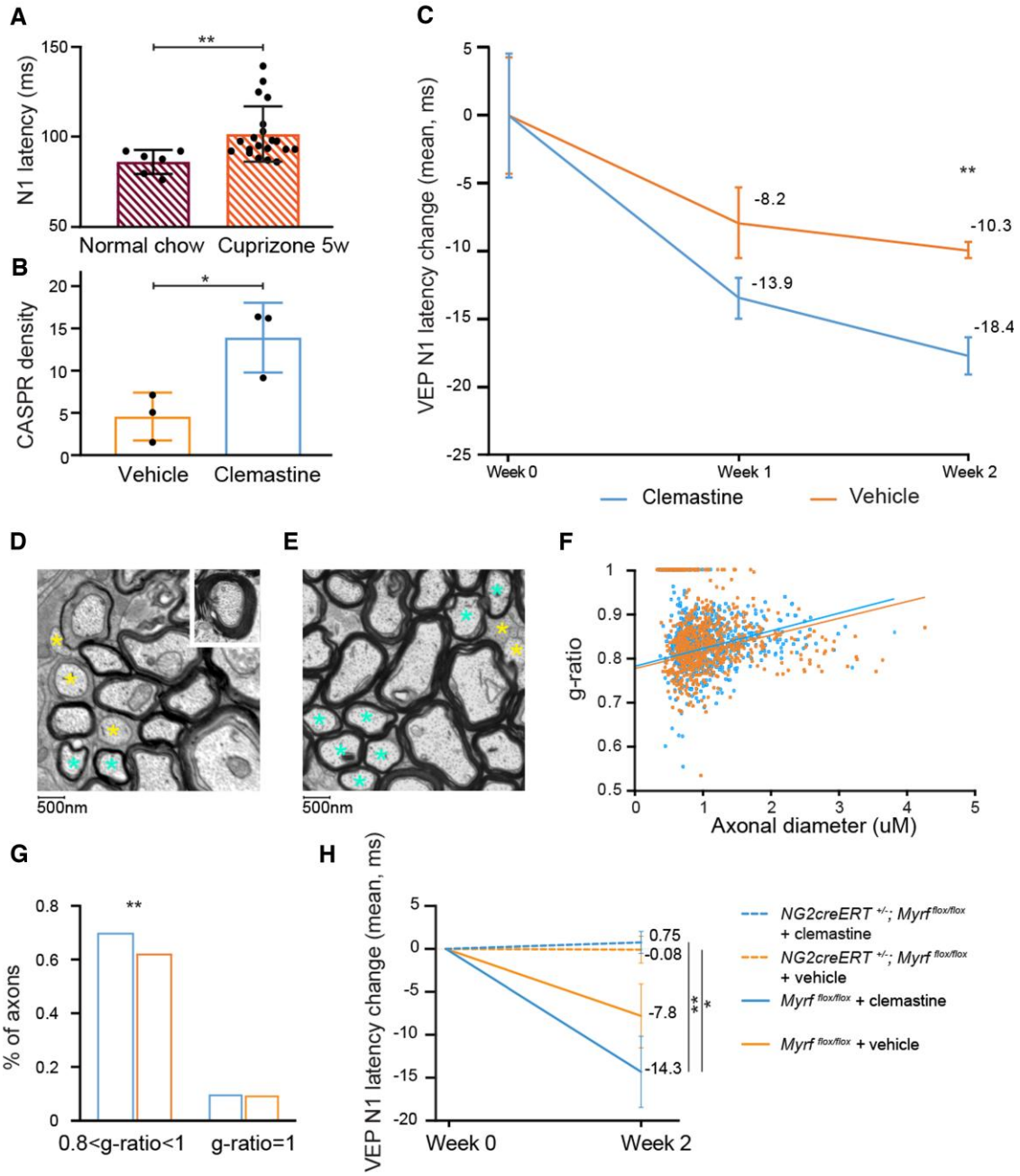

Figure 2 Effect of clemastine on remyelination after toxic demyelination by cuprizone including a model with no capacity for forming new myelin. (**A**) Cuprizone diet provokes N1 latency delay. The graph shows VEP latency in healthy subjects (average N1 = 86 ms, SD 6.7) and mice after 5 weeks of cuprizone diet (average N1 = 101.6 ms, SD 15), $P = 0.002$. (**B**) CASPR staining of ONs (5 weeks of cuprizone diet, followed by 2 weeks of treatment with clemastine/vehicle) shows a higher density (count × 10^3/mm^2) of paranodes in clemastine-treated mice. (**C**) Clemastine enhances the degree and pace of latency recovery ($P = 0.007$ at 14 days). (**D** and **E**) Examples of EM micrographs of mouse ONs after 5 weeks of cuprizone followed by 2 weeks with vehicle (**D**) or clemastine (**E**). (**F**) G-ratios of ON axons from the same experiment (five mice analysed per group). (**G**) Quantification of unmyelinated (g-ratio = 1) and remyelinating (0.8 < g-ratio < 1) axons. (**H**) Absence of improvement in delay of N1 latency after discontinuing cuprizone diet in *NG2creERT*$^{+/-}$*Myrf*$^{flox/flox}$ mice, even if treated with a remyelinating compound (clemastine). Clemastine enhances the degree and pace of latency recovery in wild-type [mean (SEM) −14.3 ms (4.1)] mice but not in *NG2creERT*$^{+/-}$*Myrf*$^{flox/flox}$ mice [mean (SEM) 0.8 ms (1.3)]. Error bars represent SEM for latency change.

model shows that VEP N1 latency in EAE is correlated with a quantitative measure of myelination (immunohistochemistry for CASPR), both in condition of optic nerve demyelination and optic nerve remyelination. VEP latency and CASPR quantification are able to capture the functional and morphological improvement related with treatment with clemastine, a remyelinating drug able to improve VEP P100 latency in RRMS patients without recent optic neuritis. We also document that cuprizone diet induces VEP delay as a consequence of visual pathway demyelination and demonstrate that VEP is a useful preclinical biomarker for testing the effect of remyelinating drugs in toxic demyelination. Our results are confirmed in both EAE and cuprizone by optic nerve ultrastructural analysis. Treatment with clemastine reduces the number of unmyelinated axons ($P < 0.01$) and increases the number of

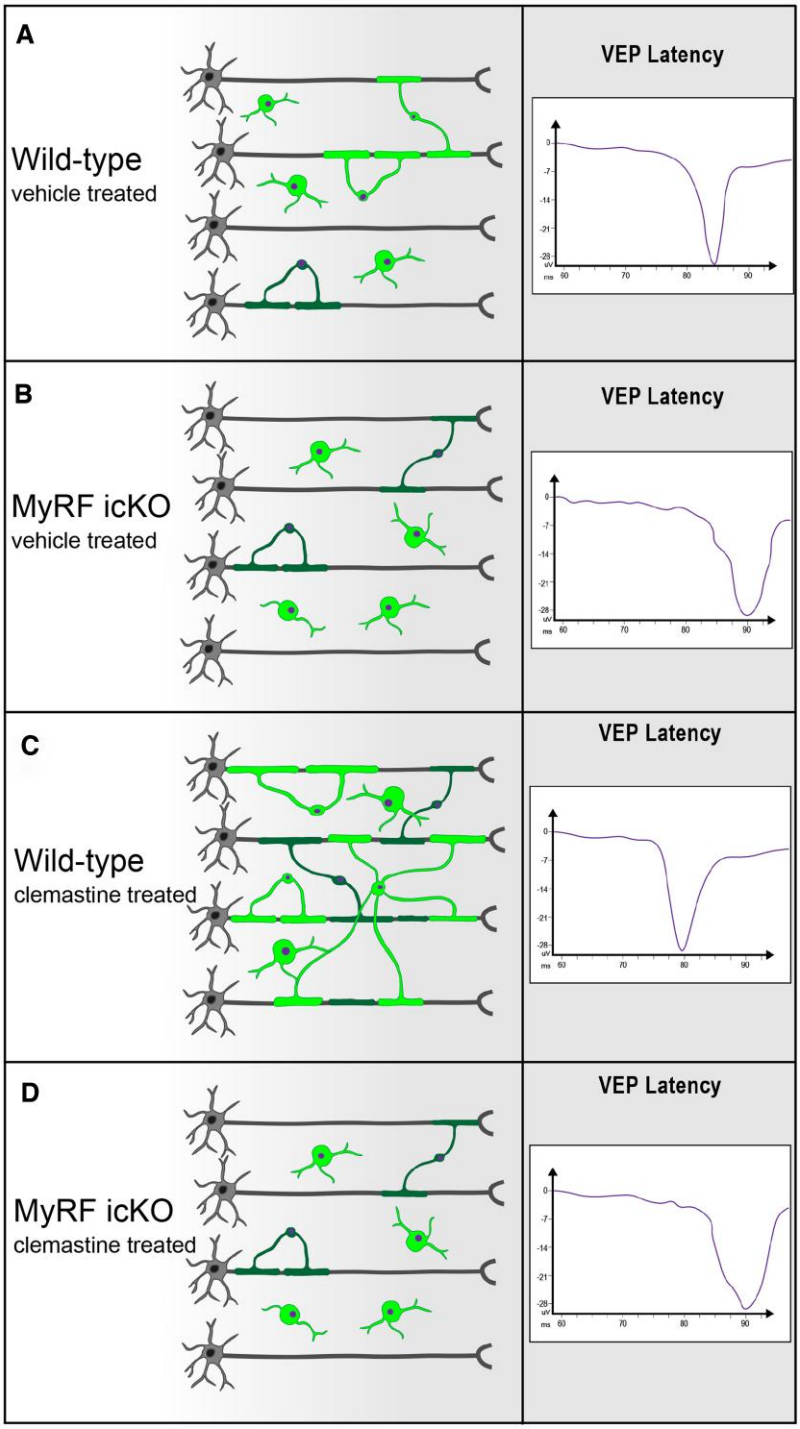

Figure 3 Schematic representation of experiment documenting the contingency of VEP improvement on remyelination. The provision of clemastine that induces OPC differentiation leads to enhanced VEP recovery following chemical demyelination with cuprizone. Blocking OPC's capacity to differentiate via the inducible conditional knockout of MyRF from oligodendrocyte lineage cells leads to complete abrogation of the capacity to recover VEP latency following cuprizone-induced demyelination. (**A**) Following cuprizone-induced demyelination for 5 weeks, spontaneous OPC differentiation and resultant remyelination leads to moderate improvement in VEP latency. Vehicle (20% kleptose, 10 ml/kg) was dosed *per os* daily. (**B**) Conditional knockout of $MyRF^{flox/flox}$ following tamoxifen dosing (300 mg tamoxifen/kg body for four consecutive days starting 7 days before the start of the cuprizone diet) in $creERT^{+}$ animals on an NG2 promoter. Vehicle-treated *MyRF icKO* animals cannot form new myelin and show no VEP latency improvement after cuprizone discontinuation. Vehicle (20% kleptose, 10 ml/kg) was dosed *per os* daily. (**C**) Daily administration of clemastine (10 mg/kg, prepared in 20% kleptose) to wild-type mice leads to increased remyelination and a significant enhancement of the improvement in VEP latency. (**D**) Despite the administration of clemastine as in **C** the enhanced recovery of VEP latency is lost in animals unable to form new myelin. This group reproduces the same results seen in condition (**B**). Clemastine was dosed *per os* daily (10 mg/kg prepared in 20% kleptose).

remyelinating axons ($P < 0.01$) in EAE and increases the number of remyelinating axons ($P < 0.01$) when administered after toxic demyelination. Our experiments blocking OPC's capacity to differentiate via the inducible conditional knockout of MyRF from NG2 cells, leading to complete abrogation of the capacity to recover VEP latency following cuprizone-induced demyelination, showed that the administration of clemastine induces VEP recovery through OPC differentiation.

Therefore, using the tools of experimental pathology, including immunohistochemical assessment of nodal architecture, detailed ultrastructural evaluation and genetic manipulation we have validated and certified VEP as a preclinical tool to measure remyelination. In addition, these data provide strong evidence that VEP is a pathologically informative end point for human clinical trials. This aligns with the concept that pathological verification of biomarkers in the preclinical setting is a crucial step for developing treatments for neurological disease. The validation of functional/behavioural outcomes such as VEP latency in mouse models of demyelination is also crucial to avoid the failure of future clinical trials (as with high-dose biotin) or relying only on biological histologic markers without functional recovery. Validation of a drug to promote OPC differentiation and myelin formation is not enough to demonstrate the restoration of proper saltatory conduction. Future studies should also address the relationship between VEP latency improvement and neuroprotection.

Funding

This study was funded by the National Institute of Health / National Institute of Neurological Disorders and Stroke (R01NS105741 grant, A.G.), the Adelson Medical Research Foundation (APND grant A130141, J.R.C.), and the Rachleff family endowment (A.R.C. and J.R.C.). C.C. was supported by the Fondazione Italiana Sclerosi Multipla (2013/B/4 grant)

Competing interests

C.C. reports grants from FISM (Italian Foundation for Multiple Sclerosis). K.S. is an employee at Pipeline Therapeutics. A.C.-H. is an employee of Prilenia Therapeutics. D.L. is an employee at Pipeline Therapeutics. J.R.C. has received research support from the National Multiple Sclerosis Society, has current support from the Adelson Medical Research Foundation and grants from the National Institutes of Health. J.R.C. has also received personal compensation for consulting from Inception Sciences (Inception 5) and Pipeline Therapeutics Inc. J.R.C. is a contributor and has received personal compensation for a US Provisional Patent Application concerning the use of bazedoxifene as a remyelination therapy (US Provisional Patent Application Serial Number 62/374270 (issued 08/12/2016). A.J.G. reports grants and other support from Inception Biosciences, other support from MedImmune/Viela, grants from the National MS Society and US National Institutes of Health, other support from Sherak Foundation, Adelson Foundation, Hilton Foundation, Pipeline Pharmaceutics, JAMA Neurology, and Bionure, outside the submitted work. A.J.G. is a contributor for a Patent Application concerning small molecule drug for remyelination. The other authors report no competing interests.

Supplementary material

Supplementary material is available at *Brain* online.

References

1. Mei F, Fancy SPJ, Shen YA, *et al*. Micropillar arrays as a high-throughput screening platform for therapeutics in multiple sclerosis. *Nat Med*. 2014;20:954–960.
2. Deshmukh VA, Tardif V, Lyssiotis CA, *et al*. A regenerative approach to the treatment of multiple sclerosis. *Nature*. 2013;502:327–332.
3. Green AJ, Gelfand JM, Cree BA, *et al*. Clemastine fumarate as a remyelinating therapy for multiple sclerosis (ReBUILD): A randomised, controlled, double-blind, crossover trial. *Lancet*. 2017;390:2481–2489.
4. Strain GM, Tedford BL. Flash and pattern reversal visual evoked potentials in C57BL/6J and B6CBAF1/J mice. *Brain Res Bull*. 1993;32:57–63.
5. Ridder WH III, Nusinowitz S. The visual evoked potential in the mouse–origins and response characteristics. *Vision Res*. 2006;46:902–913.
6. Cadavid D, Balcer L, Galetta S, *et al*. Safety and efficacy of opicinumab in acute optic neuritis (RENEW): A randomised, placebo-controlled, phase 2 trial. *Lancet Neurol*. 2017;16:189–199.
7. Brown JWL, Cunniffe NG, Prados F, *et al*. Safety and efficacy of bexarotene in patients with relapsing-remitting multiple sclerosis (CCMR One): A randomised, double-blind, placebo-controlled, parallel-group, phase 2a study. *Lancet Neurol*. 2021;20:709–720.
8. Matsunaga Y, Kezuka T, An X, *et al*. Visual functional and histopathological correlation in experimental autoimmune optic neuritis. *Invest Ophthalmol Vis Sci*. 2012;53:6964–6971.
9. Bilbool N, Kaitz M, Feinsod M, Soffer D, Abramsky O. Visual evoked potentials in experimental allergic encephalomyelitis. *J Neurol Sci*. 1983;60:105–115.
10. Onofrj M, Gambi D, Bazzano S, *et al*. Evoked potentials (EPs) in experimental allergic encephalomyelitis: A study of EP modifications during the course of a controlled disease. *Electromyogr Clin Neurophysiol*. 1992;32:125–135.
11. Balatoni B, Storch MK, Swoboda EM, *et al*. FTY720 sustains and restores neuronal function in the DA rat model of MOG-induced experimental autoimmune encephalomyelitis. *Brain Res Bull*. 2007;74:307–316.
12. Diem R, Demmer I, Boretius S, *et al*. Autoimmune optic neuritis in the common marmoset monkey: Comparison of visual evoked potentials with MRI and histopathology. *Invest Ophthalmol Vis Sci*. 2008;49:3707–3714.
13. Mozafari S, Sherafat MA, Javan M, Mirnajafi-Zadeh J, Tiraihi T. Visual evoked potentials and MBP gene expression imply endogenous myelin repair in adult rat optic nerve and chiasm following local lysolecithin induced demyelination. *Brain Res*. 2010;1351:50–56.
14. Heidari M, Radcliff AB, McLellan GJ, *et al*. Evoked potentials as a biomarker of remyelination. *Proc Natl Acad Sci U S A*. 2019;116:27074–27083.
15. Cruz-Herranz A, Dietrich M, Hilla AM, *et al*. Monitoring retinal changes with optical coherence tomography predicts neuronal loss in experimental autoimmune encephalomyelitis. *J Neuroinflammation*. 2019;16:203.
16. Mei F, Lehmann-Horn K, Shen YA, *et al*. Accelerated remyelination during inflammatory demyelination prevents axonal loss and improves functional recovery. *eLife*. 2016;5:e18246.
17. Bodini B, Veronese M, García-Lorenzo D, *et al*. Dynamic imaging of individual remyelination profiles in multiple sclerosis. *Ann Neurol*. 2016;79:726–738.
18. Bottes S, Jessberger S. Live imaging of remyelination in the adult mouse corpus callosum. *Proc Natl Acad Sci U S A*. 2021;118:e2025795118.

19. Arous J B, Binding J, Léger JF, *et al*. Single myelin fiber imaging in living rodents without labeling by deep optical coherence microscopy. *J Biomed Opt*. 2011;16:116012.
20. Farrar MJ, Wise FW, Fetcho JR, Schaffer CB. In vivo imaging of myelin in the vertebrate central nervous system using third harmonic generation microscopy. *Biophys J*. 2011;100:1362–1371.
21. Schain AJ, Hill RA, Grutzendler J. Label-free in vivo imaging of myelinated axons in health and disease with spectral confocal reflectance microscopy. *Nat Med*. 2014;20:443–449.
22. Wang H, Fu Y, Zickmund P, Shi R, Cheng JX. Coherent anti-stokes Raman scattering imaging of axonal myelin in live spinal tissues. *Biophys J*. 2005;89:581–591.
23. Osso LA, Rankin KA, Chan JR. Experience-dependent myelination following stress is mediated by the neuropeptide dynorphin. *Neuron*. 2021;109:3619–3632.e5.
24. Schmued LC. A rapid, sensitive histochemical stain for myelin in frozen brain sections. *J Histochem Cytochem*. 1990;38:717–720.
25. Rasband MN, Peles E. Mechanisms of node of Ranvier assembly. *Nat Rev Neurosci*. 2021;22:7–20.
26. Bagchi B, Al-Sabi A, Kaza S, *et al*. Disruption of myelin leads to ectopic expression of K(V)1.1 channels with abnormal conductivity of optic nerve axons in a cuprizone-induced model of demyelination. *PLoS ONE*. 2014;9:e87736.
27. Namekata K, Kimura A, Harada C, *et al*. Dock3 protects myelin in the cuprizone model for demyelination. *Cell Death Dis*. 2014;5:e1395.
28. Kojima W, Hayashi K. Changes in the axo-glial junctions of the optic nerves of cuprizone-treated mice. *Histochem Cell Biol*. 2018;149:529–536.
29. McKenzie IA, Ohayon D, Li H, *et al*. Motor skill learning requires active central myelination. *Science*. 2014;346:318–322.
30. Gold R, Linington C, Lassmann H. Understanding pathogenesis and therapy of multiple sclerosis via animal models: 70 years of merits and culprits in experimental autoimmune encephalomyelitis research. *Brain*. 2006;129:1953–1971.
31. Whitacre CC, Dowdell K, Griffin AC. Neuroendocrine influences on experimental autoimmune encephalomyelitis. *Ann N Y Acad Sci*. 1998;840:705–716.